Geoderma 299 (2017) 63–72

Contents lists available at ScienceDirect

Geoderma

journal homepage: www.elsevier.com/locate/geoderma

Gaining insights into interrill erosion processes using rare earth element tracers

X.C. Zhang[a,*], M.A. Nearing[b], J.D. Garbrecht[a]

[a] USDA-ARS Grazinglands Research Lab, 7207 West Cheyenne St., El Reno, OK 73036, USA
[b] USDA-ARS Southwest Watershed Research Center, 2000 E. Allen Rd., Tucson, AZ 85719, USA

ARTICLE INFO

Keywords:
Interrill erosion
Rare earth elements
Sediment tracer
Soil detachment
Sediment transport
Erosion-transport-deposition system

ABSTRACT

Increasing interest in developing process-based erosion models requires better understanding of the relationships among soil detachment, transportation, and deposition. The objectives are to 1) identify the limiting process between soil detachment and sediment transport for interrill erosion, 2) understand the dynamic relationships between transport and deposition by tracking sediment fate with multiple tracers, and 3) verify the effects of slope length on interrill soil erosion. Five rare earth element (REE) tracers were applied in five bands or segments to track sediment dynamics on a 10%, 4 × 4-m long uniform slope under simulated rainfall. A silt loam soil with 8% clay and 87% silt was used. Six rain events were applied, the first four with 60 mm h^{-1} and the last two with 90 mm h^{-1}. Sediment in runoff and deposition along the slope were measured. Results confirmed that interrill soil erosion was controlled by the transport process. Thus soil erodibility estimated with many interrill erosion models was actually sediment transportability. As the slope length increased, soil erosion rates initially increased and then decreased, indicating that the upper section was dominated by erosion and the lower section by transport. Raindrop-driven creeping prevailed in the upper section while flow-driven rolling dominated in the lower section. Sediment influx from upslope clearly suppressed soil detachment downslope. Moreover, the *steady state* sediment discharge from a segment was positively correlated to the amount of sediment deposited downslope from that segment, implying that 1) re-detachment, transport, and deposition occurred simultaneously in the system and 2) sediment was transported in a form of bedload, mainly rolling or creeping on interrill areas. Sediment delivery ratios of each segment tended to slightly increase downslope, suggesting the flow-driven transport was more efficient than the raindrop-driven transport. The sequence of sediment discharged from different slope positions was inconsistent with the transport-distance theory. However, interrill erosion processes vary with soil, slope, and rainfall properties, and the findings here need to be verified in different conditions.

1. Introduction

Ellison (1945, 1947) stated that soil erosion during rainfall is a complex process resulting from (1) soil detachment by raindrop impact and surface flow and (2) sediment transport by rain splash and surface flow. To better understanding and model soil erosion processes, Meyer et al. (1975) further separated upland soil erosion into rill and interrill erosion. It has been demonstrated that interrill erosion is predominantly detached by raindrop impact and transported by raindrop-impacted sheet flow (Young and Wiersma, 1973; Meyer et al., 1975; Guy et al., 1987; Kinnell, 2005). Whereas, detachment by sheet flow alone, net transport by rain splash (or air splash), and transport by sheet flow without drop impact are negligible.

It has been shown that raindrop impact is the utmost important factor driving interrill erosion. Not only does it detach soil materials but also greatly enhances sediment transport of sheet flow (Young and Wiersma, 1973; Foster, 1982; Singer and Walker, 1983; Guy et al., 1987; Zhang and Wang, 2017). Due to its double roles in interrill erosion, it is rather difficult to clearly distinguish the limiting process between soil detachment and sediment transport on interrill areas. However, such distinction is necessary because interrill sediment delivery is often set to the lesser of the transport capacity (in case of transport-limited system) and the soil detachment rate (in case of detachment-limited system) based on the modeling framework of Meyer and Wischmeier (1969).

Meyer and Harmon (1989) found that slope length had little effect on interrill sediment delivery on unrilled short sideslopes. Foster (1982) postulated that slope length had little or no effect on interrill erosion

* Corresponding author.
E-mail address: john.zhang@ars.usda.gov (X.C. Zhang).

http://dx.doi.org/10.1016/j.geoderma.2017.04.004
Received 17 January 2017; Accepted 2 April 2017
Available online 06 April 2017
0016-7061/ Published by Elsevier B.V.

per unit area. Such postulation was in line with the assertion that detachment rate by raindrop impact controlled interrill erosion rates (Lattanzi et al., 1974; Meyer et al., 1975). That is, interrill erosion is limited by raindrop detachment, and detachment by raindrop impact is largely independent of slope length on interrill areas. Gilley et al. (1985) developed an interrill erosion model that explicitly simulates the effects of water depth on both detachment by raindrop and transport by overland flow. Detachment decreases exponentially with ponding depth due to dissipation of drop energy. It generally reaches its maximum near the upper end of the hillslope and decreases with distance as runoff accumulates. On the other hand, transport capacity is assumed to increase downslope from zero at the divide as slope length increases. Taken together, the model predicts that as slope length increases, sediment delivery initially increases (transport-limited) and then decreases (detachment-limited) with downslope distance. Parsons et al. (1994) observed that higher sediment delivery occurred at times of lower splash rate in their field experiments using simulated rainfall, and argued that transport capacity could also limit interrill soil erosion at longer slope lengths. Zhang and Wang (2017) found that sediment transport was the limiting process in their interrill experiments under a wide range of rainfall intensities, slope gradients, and slope lengths in the 2-m long plots.

Foster and Meyer (1975) proposed a conceptual model of interrill sediment delivery with respect to slope steepness as follows. For low slopes, transport capacity on interrill areas could be less than detachment rate, and thus limits sediment delivery. Conversely, for steep slopes detachment rate would be smaller than transport capacity and therefore controls interrill erosion rates. Bradford and Foster (1996) simultaneously measured both rain splash and sediment delivery with a 61-cm long soil pan, and reported that the splash rate was much greater than the wash rate at the 9% slope, demonstrating that transport was the limiting process at the 9% slope.

Interrill sediment transport is a complex and multifaceted processes. Kinnell (2005, 2009) proposed six transport modes on interrill areas, i.e., by rain or air splash, raindrop-induced rolling, raindrop-induced saltation, flow-driven rolling, flow-driven saltation, and suspension. The six transport modes may occur simultaneously on interrill areas, depending on flow depth distribution, slope steepness, rainfall intensity/drop size. In general, as flow depth increases, the dominant transport modes, as suggested by Kinnell (2005, 2000), change from air splash, raindrop-induced rolling/saltation, to flow-driven rolling/saltation. For thin sheet flows that are incapable of transporting detached particles, stimulation of raindrop impact is necessary to set particles in motion in raindrop-driven transport. Deeper and faster flows, though unable to detach original soil, has the capacity to move loose/detached materials downslope in rolling/saltation with no need for raindrop stimulation (i.e., flow-driven transport). Raindrop–driven transport that is more efficient than air splash is a transport-limited system (Kinnell, 2005). Flow-driven transport is more efficient than rain-driven transport and can become a dominant system on high slopes (Kinnell, 2000). Zhang and Wang (2017) studied interrill erosion processes on different slope lengths of < 2 m and reported that (1) saltation mode was of little importance for interrill erosion due to limited flow depth, (2) raindrop-driven creeping and flow-driven rolling in the form of bedload might be the dominant modes, and (3) raindrop-driven transport was more competent than flow-driven transport in delivering sediment load, though the former might be less efficient than the latter.

Most interrill erosion studies as reviewed above deal with interrill erosion systems under wind-free conditions. The complex and multifaceted interrill erosion processes under wind-free conditions can become even more complex when wind factor is considered. As pointed out by Erpul et al. (2003, 2013), the vector physics of wind-driven rain erosion differs greatly from that of wind-free rain erosion, and interrill erosion models developed under wind-free rain conditions cannot be directly applied to erosion under wind-driven rain conditions because additional kinetic energy from blowing wind alters raindrop impact frequency, velocity, and incidence angle. This work restricted to wind-free conditions in order to simplify and isolate interrill erosion processes, and thus erosion under wind-driven rain is beyond the scope of this study.

Rare earth elements, which are the Lanthanide series with 14 similar elements, have been successfully used in studying spatial distribution of soil erosion and to track sediment movement and deposition (Tian et al., 1994; Zhang et al., 2001, 2003; Kimoto et al., 2006a, 2006b; Polyakov and Nearing, 2004; Polyakov et al., 2009). Those studies demonstrated that the rare earth element (REE) tracers are useful for understanding soil erosion dynamics such as temporal and spatial variations of soil detachment, sediment transport, and deposition over a slope or a landscape. Zhang et al. (2003) studied interrill soil erosion on a 4-m long slope at a 10% gradient, and reported that a somewhat balanced detachment-transport-deposition system might have been reached over multiple rainfall events. These results suggest that interrill erosion is a continuous process that involves simultaneous and interactive detachment, re-detachment, transport, and deposition on interrill areas. The results also demonstrate that new insights into sediment dynamics can be gained by using multiple tracers that track movement of tagged soil particles at different slope positions. Such insights would be impossible to achieve using conventional erosion measurement techniques. Thus, it is strongly recommended that sediment tracking technique be used in order to fully understand soil erosion dynamics and processes.

The general understanding of interrill erosion is that soil detachment is primarily caused by raindrop impact, and sediment delivery is mainly transported by raindrop-impacted sheet flow. However, the detailed erosion processes including the dominant erosion process and prevalent transport modes are still unclear. A better understanding of the relationships among soil detachment, transport, and deposition on interrill area is imperative for correctly interpreting experimental data and developing process-based interrill erosion models. The objectives are to 1) identify the limiting process between soil detachment and sediment transport by directly measuring sediment deposition along a uniform 10% slope over multiple simulated rainfall events, 2) characterize the dynamic relationships among detachment, re-detachment, transport, and deposition by tracking sediment source, movement, and fate with multiple tracers, and 3) understand the effects of slope length on erosion-transport-deposition systems on interrill areas. It should be pointed out that the 2003 paper of Zhang et al. was to demonstrate the usefulness of the REE tracking technique for studying soil erosion, while this paper is to extract and interpret the useful information imparted by REE tracers to gain new insights on complex relationships of erosion-transport-deposition processes on interrill areas.

2. Materials and methods

2.1. Soil and rare earth oxide characteristics

Surface soil samples of a Camden silt loam (mixed, mesic Typic Hapludalt) were collected near West Lafayette, Indiana, USA. The soil had approximately 8% clay and 87% silt. The REE background concentrations of Gd, Sm, Pr, La, and Nd elements in this soil were 2.98, 3.18, 4.38, 17.06, and 16.29 $\mu g\, g^{-1}$, respectively. Five REE oxides (La_2O_3, Pr_6O_{11}, Nd_2O_3, Sm_2O_3, and Gd_2O_3) were used. Purity and REE oxide content are shown in Table 1. Other properties can be found in Zhang et al. (2003).

2.2. Soil preparation and REE application

A runoff box (4 by 4 m) was set to a 10% slope, which, though arbitrarily, was selected in light of the existence of large erosion data at 9% slope in the literature. The soil was sieved through an 8-mm sieve and was packed into the box to a depth of 0.2 m over a 0.5-m sand layer

Table 1
Percent REE oxide content and purity.

Chemical formula	REE oxide (%)	Purity[a] (%)
Gd_2O_3	96.54	98.97
Sm_2O_3	95.91	98.14
Pr_6O_{11}	91.86	95.53
La_2O_3	80.09	98.44
Nd_2O_3	84.63	99.02

[a] REE oxide of interest divided by total of the five REE oxides.

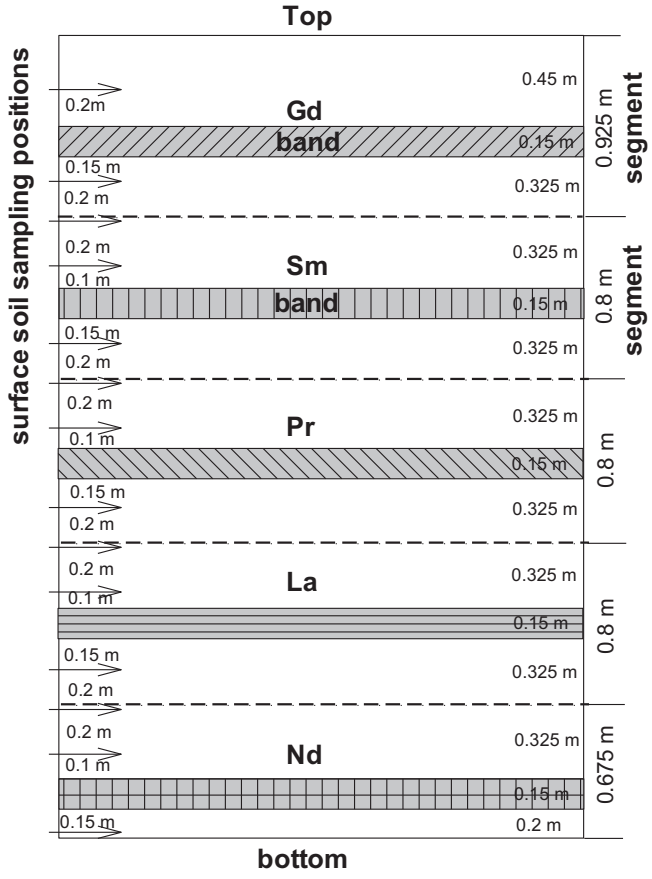

Fig. 1. Schematic layout of tracked segments, locations of tracer band placement, and soil surface sampling positions.

to ensure free drainage. The target bulk density of the packed soil was 1.3 Mg m^{-3}. The soil surface was smoothed to remove micro relief. The soil was pre-wetted before the first rain event and kept wet with trickle irrigation tubes between rainfall events.

The soil box was divided into five segments (Fig. 1), which were represented by five 0.15-m tracer bands. The top and bottom segments were 0.925 m wide and 0.675 m, respectively, with the remaining segments being 0.8 m each. The centerlines of each REE band were located at 0.525, 1.325, 2.125, 2.925, and 3.725 m from the top of the box for Gd, Sm, Pr, La, and Nd, respectively. The Sm, Pr, and La bands were centered in their segments, while the Gd and Nd bands were approximately 6 cm below the centerlines. The tracer application depths were 3 cm for the Gd, Sm, and Nd bands and 5 cm for the Pr and La bands. Soil was excavated from each band, and the excavated soil was moistened to 15 to 20% water content to facilitate REE-soil binding. The soil was then mixed with a predetermined amount of REE oxide, and the mixing was carried out in a dilute fashion to ensure homogeneity. The mixture was back-filled to the excavated depression. The doped REE concentrations in each band as well as their corresponding concentrations in each segment are shown in Table 2.

Table 2
Rare earth element (REE) concentration in each tracer band, representative REE concentration in each segment, soil background concentration, and extraction efficiency of each element.

Element	REE concentration in			Extraction efficiency %
	Tracer band μg g^{-1}	Segment μg g^{-1}	Background μg g^{-1}	
Gd	5708.2	925.7	2.98	91.43
Sm	5591.7	1070.3	3.18	86.13
Pr	5362.5	1048.4	4.38	89.35
La	4973.7	1005.5	17.06	89.30
Nd	5489.7	1268.5	16.29	92.31

2.3. Rainfall simulation and sediment collection

Rainfall simulators with oscillating type nozzles, with a spatial coefficient of variation being < 7.5%, were used to deliver six consecutive rain events at roughly 3-day intervals. The rainfall intensity was 60 mm h^{-1} for the first four rains and 90 mm h^{-1} for the last two. All rains lasted 1 h. Runoff and sediment were collected at 2-min intervals, and measured gravimetrically. To reduce the sample number for REE extraction, every three consecutive sediment samples were combined and crushed to < 2 mm for REE extraction.

2.4. Surface soil sampling

Open-ended rectangular boxes (3 × 2 cm and 1 cm deep) were used to take surface soil samples after each rain. The box was gently pushed into the soil until the top rim flushed with the soil surface. The sample was excavated, and the hole was then back filled with the blank soil. Two surface samples, taken at the same slope position and approximately 0.2 m apart, were composited. Fourteen composite samples were taken along a downslope transect at the 14 slope positions (see Fig. 1 for exact locations). The first transect was near the left sidewall of the plot, and the subsequent transects following each rain were shifted 0.3 m to right to avoid overlap of the sampling areas. Samples were air-dried and crushed to < 2 mm for REE extraction.

2.5. Rare earth element extraction and ICP-MS analysis

A quick acid leaching procedure was used to extract REEs from all soil and sediment samples. The procedure was described in detail in Zhang et al. (2003). Briefly, 2 g of soil sample was extracted with concentrated acids (HNO_3 and HCl) and H_2O_2. Two replicates were made for each sample. Dilutions of the original extract were made in triplicate for ICP-MS analysis. The overall means of the duplicate and the triplicate were used in this work. The ICP-MS sample and standard preparations as well as ICP-MS data correction can be found in Zhang et al. (2003). Extraction efficiency, expressed as the percentage of added REE that was recovered by the extracting procedure, is listed in Table 2.

2.6. Sediment REE data analysis

Sediment REE concentrations directly measured with ICP-MS need to be corrected for soil background concentration and extraction efficiency. The corrected concentration for tracer i in time step j (CC_i^j) can be computed as

$$CC_i^j = (C_i^j - B_i)/E_i \quad (1)$$

where C_i^j is the ICP-measured REE concentration of tracer i in time step j, B_i is the background concentration of tracer i, and E_i is the extraction efficiency for tracer i.

The fraction of sediment that originated from tracer or segment i

during time step j can be estimated from mass balance considerations as

$$L_i^j/T^j = CC_i^j/O_i \quad (2)$$

where L_i^j is the amount of sediment delivered from segment i during time j; T^j is the total sediment mass collected at the outlet during time j, and O_i is the original tagged or applied concentration of tracer or segment i. L_i^j can be calculated by multiplying the right hand side of Eq. (2) by T^j.

2.7. Soil REE data analysis

The extracted REE concentrations of the surface soil samples also need to be corrected for the background concentrations and extraction efficiencies to estimate CC. Again based on mass balance, deposition per sampling area (2 × 3 cm) at position k (sampling locations) from tracer or segment i after rain n (D_{ik}^n) can be computed as

$$D_{ik}^n = CC_{ik}^n \times M_k/O_i \quad (3)$$

where M_k is the sample mass from position k. Total deposition at position k from all segments or tracers upslope after rain n (D_k^n) is the sum of D_{ik}^n for all those segments. If we assume that D_k^n is representative of the average deposition rate for the area between positions $k-1$ and $k+1$, the overall total deposition along the entire slope profile after rain n (D^n) is

$$D^n = \sum (D_k^n \times A_k) \text{ for all } k \quad (4)$$

where A_k is the representative area of position k. For better representativeness, the attempt was made to center A_k around position k as much as possible. Note total deposition was the cumulative deposition from the first rain to the rain in question. Thus, net deposition or re-detachment per rain is the difference of D^n and D^{n-1}.

Sediment delivery ratio for a rain event is defined as the ratio of sediment discharged to the outlet to the sum of the discharged sediment and deposition on the slope during that event. If we assume that deposition from the previous rain was re-detached and re-transported during each subsequent rain, sediment delivery ratio for rain n (ρ^n) may be estimated by

$$\rho^n = Y^n/(Y^n + D^n) \quad (5)$$

where Y^n is the measured total sediment discharge during rain n. This equation is also applicable to estimate sediment delivery ratio for each segment (ρ_i^n), if the total sediment discharge (Y_i^n) and deposition (D_i^n) from segment i are used instead. Furthermore, sediment delivery ratio over multiple rain events (ρ_m^n) can be estimated as

$$\rho_m^n = \sum Y^n/(\sum Y^n + D^n) \quad (6)$$

where ΣY^n is the sum of discharged sediment from rain 1 to rain n. The long-term sediment delivery ratio over multiple rains is actually a better representation of the sediment budget of the system in question.

It should be pointed out that all the estimation equations can be applied either to each segment or tracer band only (Fig. 1), using the respective tracer concentrations in Table 2 as well as their representative areas.

3. Results

Runoff and sediment discharge rates are plotted with elapsed time for all six rain events in Fig. 2. Runoff initiated at the 15 min mark during the first rain, and gradually increased to the steady state level by the 45 min mark (Fig. 2A). Runoff started about 2 min into the rainfall event for all subsequent rain events, and reached the steady state levels rather rapidly. The steady state runoff rates corresponded well with the rainfall intensities, which were 60 mm h^{-1} for the first four rain events and 90 mm h^{-1} for the last two rain events. The changes in runoff rates between rain events provide a unique opportunity to study changes in

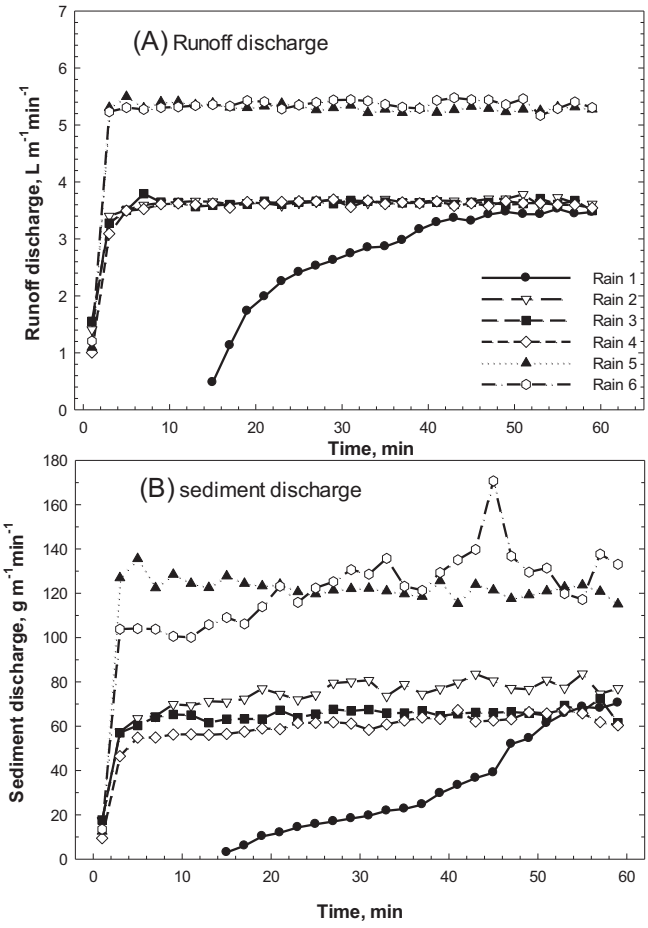

Fig. 2. Surface runoff and sediment discharges over time for the six rainfall events.

erosion regimes and erosion dynamics regarding the relative importance of soil detachment, sediment transport, and deposition, as affected by rainfall intensity and flow depth. Sediment discharge rates, though more variable in time and between rainfall events, corresponded well with runoff rates (Fig. 2B). Sediment discharge increased gradually in the first rain and reached the quasi-steady state level by the end. Sediment discharge rates reached the quasi-steady state levels within a few minutes into each subsequent rain event and remained more or less constant throughout each event.

REE-derived fractional sediment discharges from each segment over time are shown in Fig. 3 for all rain events. The summations of all fractional contributions were slightly greater than one in the early stages of rain events 1 and 2, due to the tracking errors resulting from REE measurement error and selective erosion (Zhang et al., 2003). Overall, sediment contributions from each segment were fairly stable throughout each rain except La in rain events 1, 5, and 6, with the proportions contributed from each segment gradually evolving between rain events. In rain event 1 the proportions of sediment from the La segment at the runoff initiation stage were very high due to its proximity to the outlet (though total sediment discharge was very low at the stage) and preferred transport of fines, and rapidly decreased to the steady stage level of 0.1. In rain events 5 and 6 the contributing proportions from the La segment increased rapidly near the ends due to the initiation of micro-rills under the high rainfall intensity of 90 mm h^{-1}. Although a few micro-rills occurred in the lower section of the plot in rains 5 and 6, interrill erosion process dominated this experiment for most time and on most parts of the plot. Generally, most soil loss in rain 1 was from the Pr segment, and followed by Sm. The contributions from Pr and Sm were about equal in rain event 2 with a considerable increase from Gd, indicating that the locus of the max-

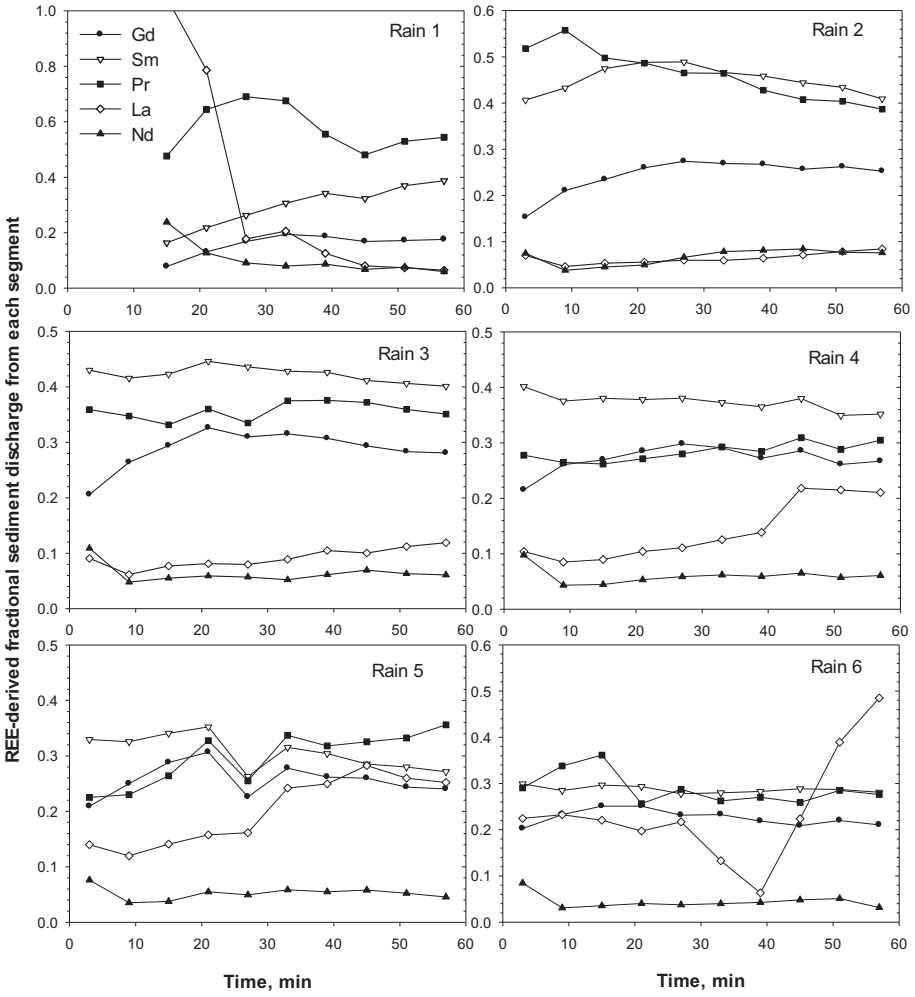

Fig. 3. Temporal changes of REE-derived fractional sediment contributions from each segment for the six rainfall events.

imum erosion migrated upslope. The upslope migration of the locus continued in rain events 3 and 4 under the same rainfall intensity of 60 mm h^{-1} with the contributions from Sm surpassing those from Pr. Interestingly, the contributions from the upper three segments of Sm, Pr, and Gd were similar in rain events 5 and 6 under the increased rainfall intensity of 90 mm h^{-1}, indicating that severe soil erosion was occurring in the upper three segments. The trend was very clear that the erosion contributions from the lowest Nd segment were smallest for all six rain events, suggesting sediment transport process dominated in the segment near the outlet.

Soil loss rates per unit area estimated for different slope lengths are plotted with downslope distance in Fig. 4. Similar downslope trends of soil loss rates are shown for both event total (Fig. 4A) and quasi-steady state rates (Fig. 4B). That is, soil loss rates averaged over different slope lengths increased with downslope distance, peaked near the middle of the plot, and then decreased with distance to the outlet. The greatest erosion rates per unit area per event occurred at the slope length of 2.5 m for all six rain events except rain event 4 in which it occurred at the length of 1.7 m (Fig. 4A). The greatest “steady state” erosion rates per unit area also occurred at the slope length of 2.5 m for all six rain events except rain event 6 in which it occurred at the length of 3.3 m (Fig. 4B). Because of the formation of micro-rills in the La segment near the ends of rain event 6, the maximum erosion rates migrated downslope. The micro-rill erosion was not the focus of this study but was presented for entirety. Cumulative downslope soil loss amounts per event are shown in Fig. 5 for all rain events. Cumulative soil loss increased nearly linearly with distance between 0 and 2.5 m for all rain events. However, the rates of the increases decreased considerably between 2.5 and 4 m. The lesser decreases in rain events 5 and 6 were largely caused by the increased transport capacity due to the increased rainfall intensity, suggesting sediment transport process might have limited the sediment delivery in the system.

Total sediment discharges per unit width from each segment are shown in Fig. 6A for all six rain events. The cumulative soil losses over the six rain events were mostly from the Sm and Pr segments, followed by the Gd and then La segments, with the least from the Nd segment, indicating that the upper three segments were in an erosion-dominant regime while the lower two segments (especially Nd) were in a transport-dominant regime. Total amounts of the downslope deposition from each segment per unit width over the six rain events are shown in Fig. 6B. Most deposition was from the Sm segment, followed by the Pr and Gd segments and then by the La segment, with the very small amount from the lowest Nd segment. The trivial deposition from the Nd segment would otherwise indicate efficient sediment delivery from the segment due to its proximity to the outlet. However, the small amount sediment discharged from the segment in Fig. 6A suggested the opposite, indicating that this segment functioned mainly as a conduit of transporting sediment from the segments above because flow energy was mostly used for sediment transport rather than detachment. Interestingly, the amounts of deposition from each segment were well correlated with the amounts of total sediment discharged to the outlet from each respective segment. This seemingly contradictory relationship was further verified by comparing the downslope depositions from each segment following each rain with the quasi-steady state sediment discharge rates from each respective segment for all six rain events (Fig. 7). A linear relationship was obtained between the two with a

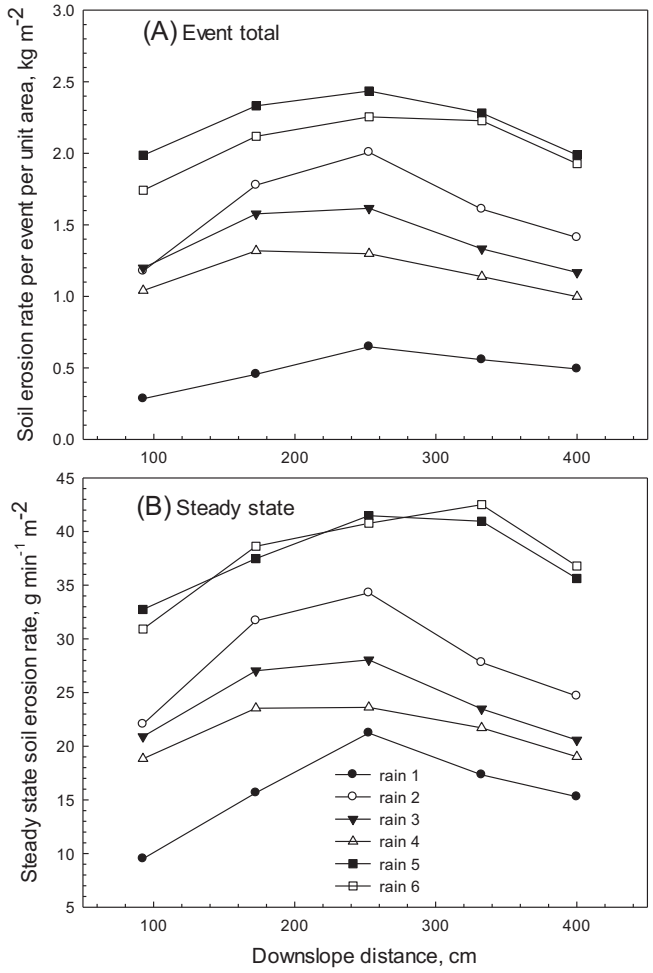

Fig. 4. Soil erosion rates per unit area calculated for each slope length (0.9, 1.7, 2.5, 3.3, and 4 m) for event total (A) and steady state rates (B).

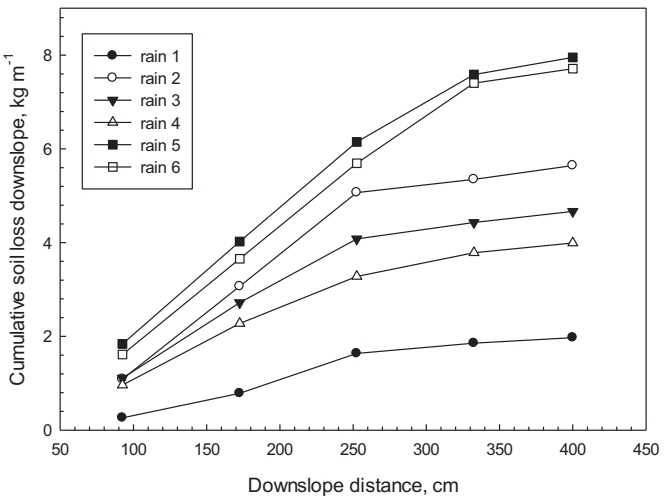

Fig. 5. Cumulative soil loss from each segment or sediment discharge downslope along the slope profile.

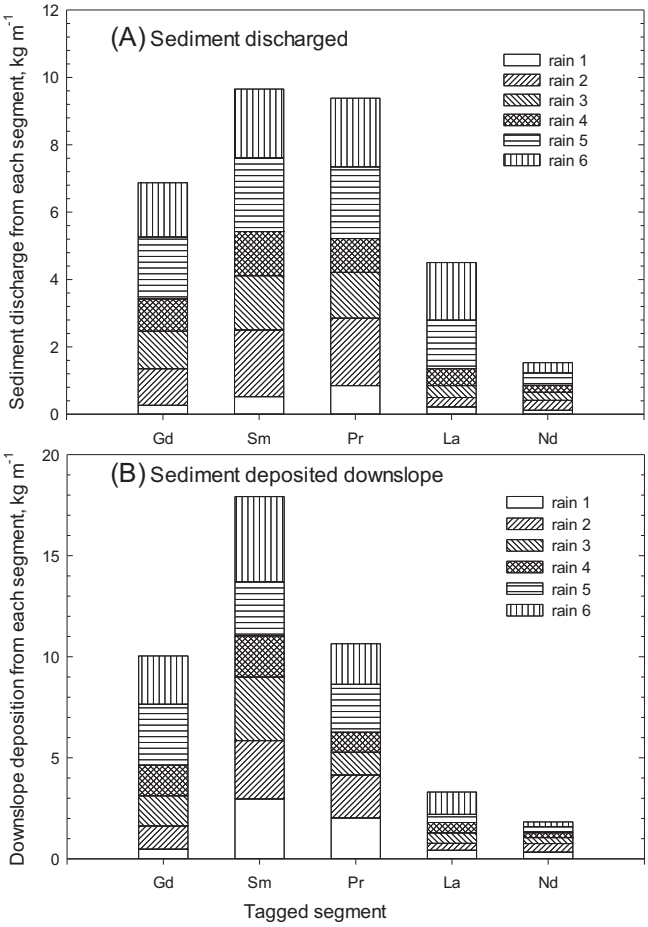

Fig. 6. Event-total sediment discharge from each segment (A) and total downslope deposition from each segment (B) for the six rainfall events.

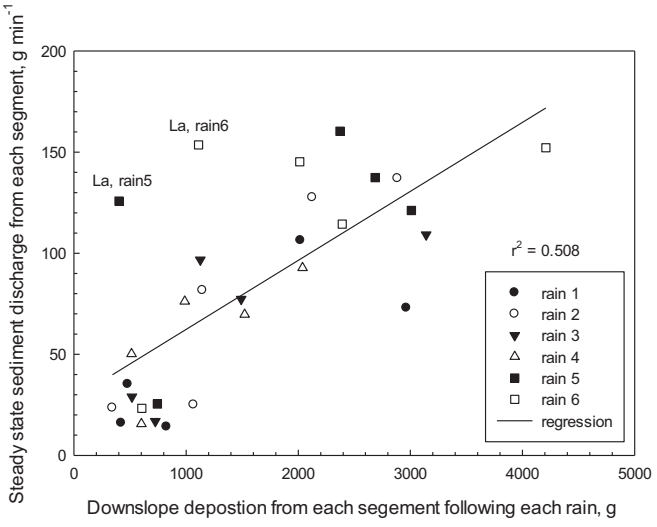

Fig. 7. Relationship between steady state sediment discharge from each segment and total downslope deposition from the same segment following each rain for all segments and rainfall events.

linear correlation coefficient of 0.713. As mentioned earlier, micro-rills were formed in the La segment in rain events 5 and 6, which expectedly showed very high sediment discharge rates but very low deposition rates (Fig. 7). The correlation coefficient increased to 0.84 without these two data points. This good relationship might indicate that the downslope depositions from each segment following each rain were in dynamic balances with the sediment delivery rates, possibly reflecting a snapshot of the steady state depositions. It should be mentioned that the coefficient of variation (CV) of measured tracer concentrations between two surface soil samples following each rain was relatively small. For example, the CVs for Gd tracer were mostly < 5% along each downslope transect following each rain, with a maximum of 28%, indicating

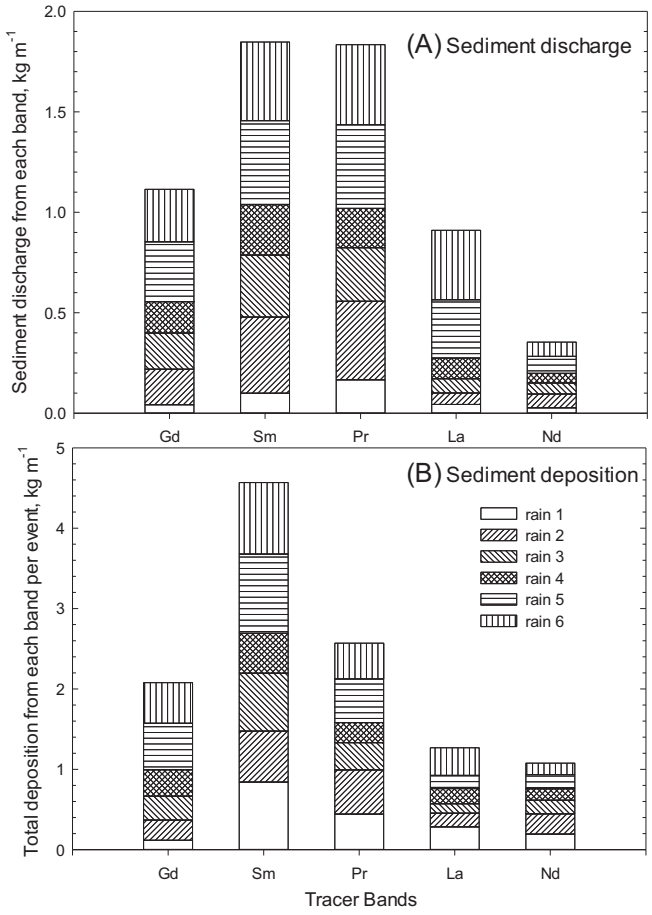

Fig. 8. Event-total sediment discharge from each band (A) and total deposition including upslope splash from each band (B) for the six rainfall events.

that sediment deposition was fairly uniform along each contour line or across the slope.

To further confirm the positive correlation between sediment deposition and sediment delivery, sediment dynamics were also investigated for the directly tagged soil in the tracer band instead of the whole segment as presented in the previous paragraph. This approach would eliminate the upscaling error of representing the whole segment with the band area (Fig. 1). The sediment discharged to the outlet from each band and the sediment deposited downslope from each band are shown in Fig. 8 for all six rain events. The markedly similar patterns between the segment-based (Fig. 6) and the band-based results indicated that the errors of representing the whole segment with the band area were relatively small, confirming that the positive correlation obtained using the segment-based estimates was reliable. Compared with the amount of sediment delivered, the relatively less deposition downslope from the Pr band was likely caused by the formation of micro-rills in the lower section of the plot, which were more efficient in transporting the influx sediment.

Sediment deposition rates from each tracer band at all 14 surface sampling points are shown in Fig. 9 for six rains. Sediment deposition rates below each tracer band were much greater than those immediately above the band. The deposition above the band was caused by air splash transport, while the deposition below the band resulted from both air splash and downslope wash by raindrop-impacted sheet flow. The wash transport tended to diminish upslope deposition by air splash while enhancing the downslope deposition from each band. The enormous differences in deposition rates between the upslope position (10 cm above each band) and the downslope position (15 cm below) indicated the dominant role of drop-impacted sheet wash in sediment transport on interrill erosion areas because net downslope splash transport has been reported to be negligible (Young and Wiersma, 1973; Kinnell, 2005). It is important to note that the sediment deposition rates along the slope were seldom uniform, and fluctuation of the highs and lows would suggest that sediment transport by raindrop-impacted sheet flow was largely in the form of bedload that roll or creep downwards in pulses or bursts.

Sediment delivery ratios of each segment during each rain were calculated using Eq. (5) (Fig. 10A). Sediment delivery ratio of rain 1 was about 0.24, which was much smaller than the mean of the remaining rain events due to the later runoff initiation, lower runoff rates during rain 1 (Fig. 2), and buildup of downslope deposition to reach deposition-transport equilibrium. The sediment delivery ratios in rain events 2 to 6 were generally similar, with a mean around 0.44 (i.e., 56% of detached sediment was deposited on the slope), indicating that sediment transport might have limited interrill erosion rates. Generally, the sediment delivery ratios from each segment seemed to increase slightly downslope as slope length increases. This increasing tendency might indicate increases in sediment transport efficiency due to the increases in flow depth and the formation of flow lines in the lower section of the plot. This might well be the case in rain events 5 and 6 for the La segment where micro-rills had formed, resulting in greater sediment delivery ratios for the segment. Likewise sediment delivery ratios were estimated for each band without upscaling (Fig. 10B). Overall the changes of sediment delivery ratios over slope position were very similar between the segment-based and band-based estimates. The slightly smaller values for the band-based estimates were partially because the upslope splash deposition from each band was included in the total deposition. In addition, cumulative sediment delivery ratios, calculated for multiple rains using Eq. (6), were 0.24, 0.52, 0.65, 0.75, 0.73, and 0.76 for rain events 1 to 6, respectively, showing that sediment delivery ratio for interrill erosion depends on time. Given a steady state erosion-transport-deposition system, the longer the rainfall event, the greater proportion of sediment would be delivered to the outlet. As a result, sediment delivery ratio increases with rainfall duration or number of rainfall events.

4. Discussion

Contradiction exists in the literature on whether soil detachment or sediment transport process actually limits interrill erosion rates. Identifying the limiting process is critical because erosion rate is often set to the rate of the limiting process (Meyer and Wischmeier, 1969). Lattanzi et al. (1974) and Meyer et al. (1975) proposed that interrill erosion was limited by soil detachment. Gilley et al. (1985) reported that transport limited erosion on shorter slopes, while detachment limited on longer slopes. Zhang and Wang (2017) simultaneously measured soil splash (or detachment) and sediment discharge under various rainfall intensities, slope gradients, and slope lengths. By comparing the splash rates and sediment discharge rates, they concluded that sediment transport was the limiting process for interrill erosion under the study conditions. This conclusion was corroborated by the results of this study. The occurrence of sediment deposition along the entire slope especially the upslope splash deposition (Fig. 9), accompanied by the sediment delivery ratios of < 0.8 for all slope segments (Fig. 10A), supported the conclusion that sediment transport was the limiting process for interrill erosion. Furthermore, the sediment discharge first increased and then decreased as slope length increased from 0 to 4 m (Fig. 4), indicating that sediment transport capacity controlled the total sediment discharge from the plot, provided that detachment by raindrop impact was similar along the slope. Flow depth and velocity were not measured in this study. However, an average flow depth of < 0.6 mm near the outlet in this study could be inferred from a similar study of Zhang and Wang (2017). Therefore, it was acceptable to assume that the effect of water depth on soil detachment by raindrop was negligible in this experiment. Given the assumed constant rate of

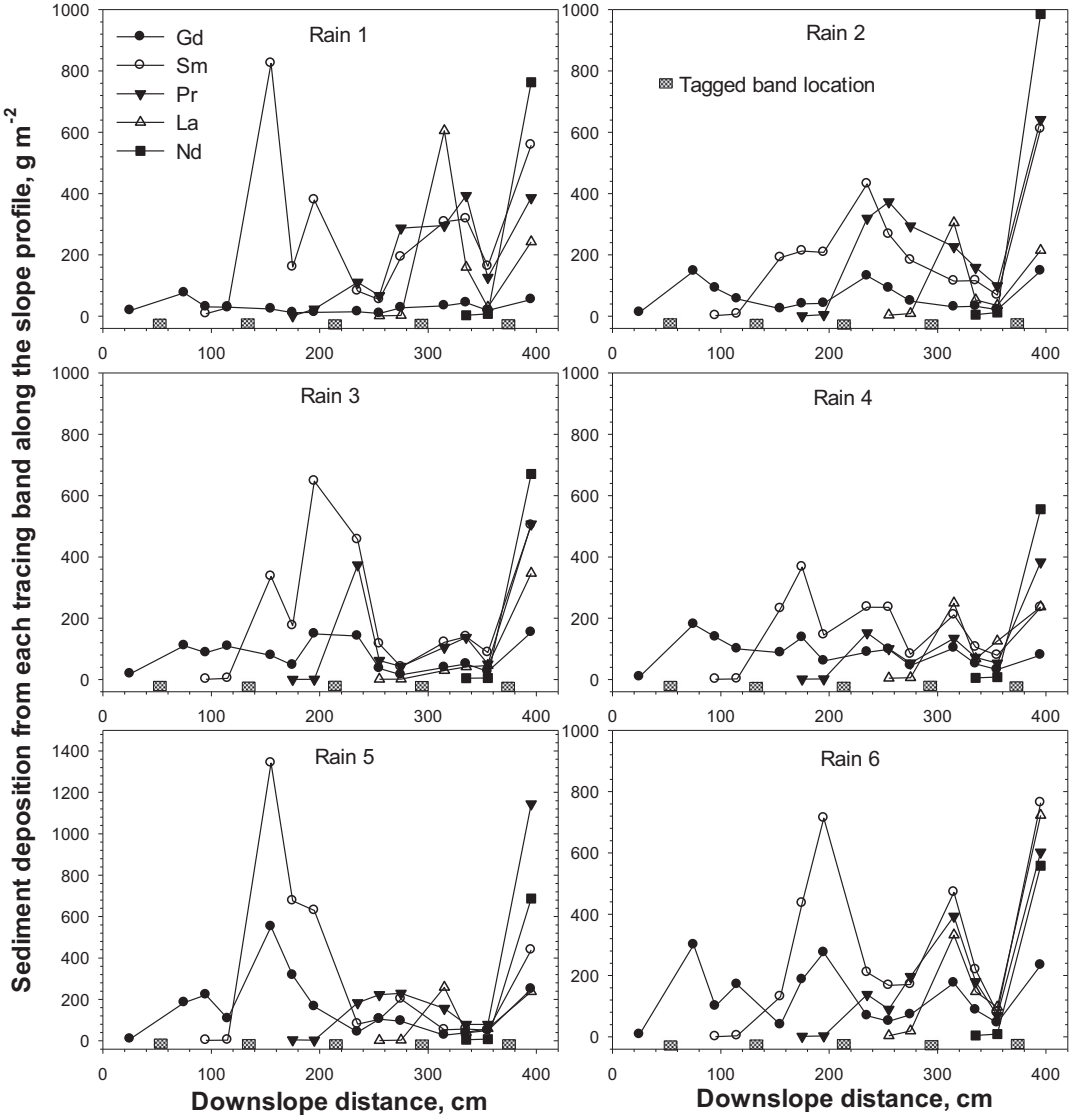

Fig. 9. Sediment deposition rates from each tracer band along the slope following each of the six rainfall events.

soil detachment by raindrop on the entire plot, the nonlinear change of sediment discharge along the slope in Fig. 4 must have resulted from changes in sediment transport capacity. If the interrill erosion was controlled by the raindrop detachment rate, the soil loss per unit area should be constant with slope length in Fig. 4. As flow depth increased downslope, sediment transport gradually transitioned from rainfall-driven mode to flow-driven mode. The former had higher sediment concentration and was more competent than the latter in transporting sediment (Zhang and Wang, 2017), although the latter was more efficient in transporting sediment due to increased flow velocity (Kinnell, 2005). The greater competence of the rainfall-driven transport was largely caused by greater enhancement of transport capacity by raindrop impact due to lower energy dissipation by smaller flow depth.

Sediment delivery per unit width increased linearly with downslope distance if the length was < 2.5 m, and then deviated from the linear relationship as slope length further increased (Fig. 5). Similar patterns were observed by Zhang and Wang (2017), who attributed the deviation to the changes in sediment transport modes. They reported that on interrill areas rainfall-driven rolling/creeping dominated in the upper section where flow depth was shallow, while flow-driven rolling/sliding became dominant in the lower section as flow depth increased. They found that sediment concentration decreased with downslope distance as sediment transport transitioned from rainfall-driven to flow-driven modes. Greater sediment concentration would signify greater competence of the flow to transport sediment. The greater competence was largely resulted from greater raindrop impacts due to smaller water depth in the upper section. The experimental results obtained here could also support the two transport modes observed by Zhang and Wang (2017). The observation indicated that rainfall-driven rolling dominated in the upper slope where near linear increases in sediment discharge existed, while flow-driven rolling prevailed in the lower slope where slopes of lesser than linear increases were exhibited (Fig. 5). The faster increases in sediment load in the upper slope were because rainfall-driven transport was more competent than flow-driven transport in transporting sediment on interrill areas.

Since sediment dynamics reached quasi-steady states near the end of each rain, a snap shot of a system should reflect the state of the system of any time. Based on this notion, sediment deposition from each segment following each rain was compared to the quasi-steady state sediment delivery rates, and a strong positive correlation was obtained in this study. The positive correlation between steady state deposition amounts and steady state sediment discharge rates would indicate that sediment re-detachment, transport, and deposition occurred simultaneously in the system. This was only possible if sediment was

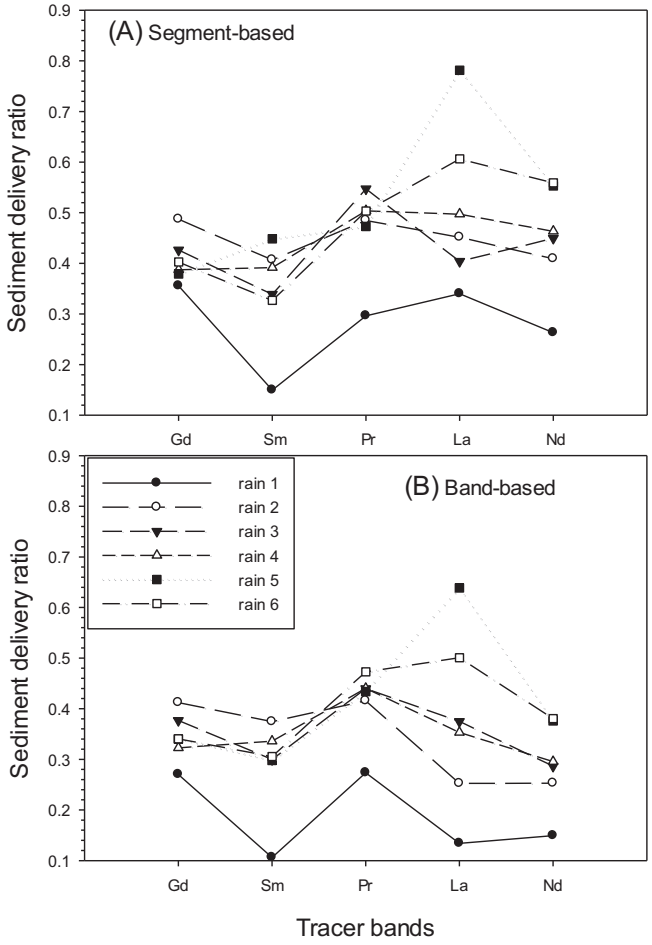

Fig. 10. Sediment delivery ratios calculated based on the entire segment (A) and the banded area only (B).

transported as bedload in the form of rolling or creeping. This inference is consistent with the empirical observations reported in the literature that interrill erosion is dominated by rolling or sliding along the surface akin to the movement of bedload (Parsons et al., 1993; Asadi et al., 2007; Wainwright et al., 2008; Zhang and Wang, 2017). Sutherland et al. (1996) reported that sediment on interrill areas was transported in a series of pulses in the form of periodic migrating bedload waves. In the rolling/creeping mode, sediment delivery rates would be positively related to transient deposition rates. The rate of the rainfall-driven creeping would be heavily influenced by the frequency of raindrop impacts and the drop sizes. The results also showed that the rate of the rolling was not uniform in time and space, but rather occurred in pulses and waves as affected by changes in rainfall intensity and drop direction, micro-relief, and flow depth or line (Fig. 9). The detailed process may be further verified with a high speed video camera.

Event sediment delivery ratio varied with runoff rate and runoff duration (Fig. 10). It also tended to increase with downslope distance due to changes in runoff rate, flow depth, and sediment transport mode. Flow-driven transport, which was more efficient than rainfall-driven transport (Kinnell, 2005), tended to yield higher sediment delivery ratios. Event sediment delivery ratio was calculated based on the transient steady state deposition and event total sediment discharge. Thus, it is a time-dependent quantity. As rainfall duration increases, estimated event sediment delivery ratio increases as total sediment discharge increases while the 'steady state' deposition rates remains somewhat unchanged. This has been verified with the sediment delivery ratio over multiple rainfall events, which increased from 0.24 in rain event 1 to 0.76 in rain event 6. This result indicates that the sediment delivery ratio concept is more useful at a longer time scale or at a larger watershed scale, where a relative stable state of the watershed can be well represented.

Foster and Meyer (1972) proposed a sediment feedback concept, stating that sediment detachment rate is inversely related to sediment load in a flow. This is based on the idea that flow energy is finite, and energy that is used for sediment transport will not be available for detachment or re-detachment. This concept implies that detachment or erosion may dominate in upper slope section where sediment load is normally low due to limited sediment influx from upslope, while sediment transport may dominate in lower section where sediment load is high. The results of this study clearly supported the concept that erosion dominated in the upper section while transport dominated in the lower section (Fig. 6A). Although sediment transport capacity increased continuously downslope as flow accumulated (Fig. 5), the rates of the increases declined as slope length increased because the enhancement of drop impact on transport capacity diminished due to flow depth increases. Thus, the lesser increases in transport capacity on interrill areas would result in lesser soil detachment from the lower section, especially in the Nd segment near the outlet. The plot end plate might have abetted sediment deposition in the Nd segment, but it is yet a proof that soil detachment is positively related to the sediment deficit (the difference between transport capacity and sediment load). Wainwright et al. (2008) questioned the validity of the sediment feedback concept and stated that the concept was based on unpublished empirical observations and not yet verified by experimental data. Nevertheless, the results from this experimental study demonstrate that the sediment feedback relationship in principle holds under conditions of dominant flow-driven transport on interill areas. This conclusion was also supported by the experimental data of Zhang and Wang (2017) who quantified soil erosion and deposition on slopes using four different slope lengths.

This study confirms the findings of Zhang and Wang (2017) that interrill soil erosion is controlled by sediment transport process rather than by raindrop detachment process on the interrill areas, as evidenced by the occurrence of steady state sediment deposition along the entire slope including the upslope splash deposition (Fig. 9) and the < 0.8 of sediment delivery ratio on the slope (Fig. 10). As widely reported in the literature, the interrill erodibility parameter (K_i) was often estimated using lumped empirical equations such as that used in the Water Erosion Prediction Project (WEPP) model. If sediment transport is the limiting process in interrill erosion as reported here, the interrill erodibility estimated with those lumped equations indeed reflects sediment transportability rather than soil erodibility. This distinction is important if interrill erosion process and soil erodibility are to be correctly represented and modeled.

An alternative erosion modeling approach based on particle-travel distance has been proposed and developed in the literature (Kirkby, 1991; Parsons et al., 1993, 1994, 2004, 2006; Wainwright et al., 2008). The approach determines erosion rates based on entrainment rates and travel distances of individual particles. It explicitly addresses the depositional process during sediment transport and shows the potential to scale soil erosion from plot to landscape (Wainwright et al., 2008). Parsons et al. (2004) developed an analytical solution for interrill erosion on a plan-planar hillslope of uniform gradient. The estimated erosion rates per unit area followed an upward-convex shape within the top 4-m slope length. The relationships between erosion rates and slope length agreed qualitatively with those obtained in this study.

Parsons et al. (1993) reported that transport distances in interrill erosion followed a negative exponential or gamma distribution, meaning that most sediment would have been deposited after travelling very short distances, normally < 1 m on average. As a result, sediment entrained only near the outlet would have been transported out of the plot. The sediment deposition rates measured along the slope appeared to be consistent with the nature of the deposition predicted by the theory. However, the discrepancy existed between the loci of maximum

soil loss on the slope. The measured maximum erosion occurred in the upper section (mainly the Sm and Pr segments); whereas the theory would predict that most soil loss be from the areas near the outlet (Parsons et al., 1994, 2006), which was also suggested by Rejman et al. (1999) based on their field experiments of different slope lengths. In addition, based on the travel distance theory, sediment discharged to the outlet should follow the proximity sequence of Nd, La, Pr, Sm, and Gd during rain 1 (Fig. 1). However, the predicted sequence was not clearly seen in the measured data in rain 1 (Fig. 3), probably because the suspension transport of fines during the runoff initiation phase might have obscured the sequence. Since the travel distance varies with particle size and flow hydraulics such as flow velocity and shear stress, a rigorous test of the applicability of the theory necessitates measurements of sediment properties and flow hydraulics. Unfortunately, these parameters were not measured in this study, and thus a thorough evaluation cannot be made here. However, since the REE-tracing technique traces movement of particles from different known source areas, it, in conjunction with measurements of sediment properties and flow hydraulics, can provide an ideal means for validating or invalidating the ability of the approach to predict sediment fluxes and depositions at different distances along a slope. As noted by Parsons et al. (2004), data on sediment fluxes at different distances were few, and such data scarcity greatly hampered the validation and development of the process-based erosion models. Undoubtedly the REE-tracing technique will provide the much needed spatial data for rigorously testing the transport-distance theory as well as other process-based models.

5. Conclusions

Development and validation of process-based erosion models necessitate better understanding of the relationships among soil detachment, sediment transportation, and deposition. Five REE tracers were used to study sediment dynamics under simulated rainfall on a 4-m long, 10% uniform slope. This study focused on the interrill erosion process; however, micro-rills did occur in the lower slope section during rains 5 and 6, which was included in the paper for entirety. The results confirmed that interrill soil erosion was limited by transport process. An upward-convex relationship existed between cumulative sediment discharge per unit width and downslope distances. Raindrop-driven rolling/creeping and flow-driven rolling/gliding were dominant transport modes for interrill erosion. The observation showed that the former dominated in upper slope section due to thin water depth, while the latter dominated in lower section. Consequently, the upper section was dominated by erosion due to limited sediment influx, and the lower section by transport largely serving as a conduit for influx sediment from upslope. The experimental data strongly supported the sediment feedback concept, showing that sediment influx from upslope clearly suppressed soil detachment downslope. More importantly, strong positive correlation was found between the amount of sediment discharged from a segment to the outlet and the amount of sediment deposited downslope from that segment, implying that sediment re-detachment, transport, and deposition occurred simultaneously in the system. The concurrent transport and deposition demonstrated that sediment was transported as bedload in the form of rolling/creeping. Sediment saltation was believed unimportant due to limited flow depth on such short slopes. Sediment delivery ratios estimated for each slope segment tended to slightly increase downslope, suggesting the flow-driven transport in the lower section was more efficient than the raindrop-driven transport in the upper section. In conjunction with measurements of sediment properties and flow hydraulics, the tracking technique will provide a unique opportunity to generate much needed spatial erosion data for validating the transport-distance theory as well as other process-based erosion models. It should be noted that the conclusion obtained from this study needs to be further verified for different soils under different slope and rainfall conditions because interrill erosion processes are strongly influenced by these factors.

References

Asadi, H., Ghadiri, H., Rose, C.W., Rouhipour, H., 2007. Interrill soil erosion processes and their interaction on low slopes. Earth Surf. Process. Landf. 32, 711–724.

Bradford, J.M., Foster, G.R., 1996. Interrill soil erosion and slope steepness factors. Soil Sci. Soc. Am. J. 60, 909–915.

Ellison, W.D., 1945. Some effects of raindrops and surface flow on soil erosion and infiltration. Trans. Am. Geophys. Union 26, 415–429.

Ellison, W.D., 1947. Soil erosion studies. Agric. Eng. 28 (145-146, 197-201, 245-248, 297-300, 349-351, 402-405, 442-444).

Erpul, G., Norton, L.D., Gabriels, D., 2003. Sediment transport from interrill areas under wind-driven rain. J. Hydrol. 276, 184–197.

Erpul, G., Gabriels, D., Norton, D., Flanagan, D.C., Huang, C., Visser, S.M., 2013. Mechanics of interrill erosion with wind-driven rain. Earth Surf. Process. Landf. 38 (2), 160–168.

Foster, G.R., Meyer, L.D., 1972. A closed-form soil erosion equation for upland areas. In: Shen, H.W. (Ed.), Sedimentation. Colorado State University, Fort Collins, Co., pp. 12.1–12.19.

Foster, G.R., 1982. Modelling the soil erosion process. In: Haan, C.T., Johnson, H.P., Brakensiek, D.L. (Eds.), Hydrologic Modeling of Small Watersheds. ASAE: St. Joseph, MI, pp. 297–382 (Chaper 8).

Foster, G.R., Meyer, L.D., 1975. Mathematical simulation of upland erosion by fundamental erosion mechanics. In: Present and Prospective Technology for Predicting Sediment Yields and Sources. ARS-S-40, USDA-ARS, U.S. Gov. Print. Office, Washington, DC.

Gilley, J.E., Woolhiser, D.A., McWhorter, D.B., 1985. Interrill soil erosion-part I: development of model equations. Trans. ASAE 28 (147–153), 159.

Guy, B.T., Dickinson, W.T., Rudra, R.P., 1987. The roles of rainfall and runoff in the sediment transport capacity of interrill flow. Trans. ASAE 30, 1378–1386.

Lattanzi, A.R., Meyer, L.D., Baumgardner, M.F., 1974. Influence of mulch rate and slope steepness on interrill erosion. Soil Sci. Soc. Am. Proc. 38, 946–950.

Kimoto, A., Nearing, M.A., Zhang, X.C., Powell, D.M., 2006a. Applicability of rare earth element oxides as a sediment tracer for coarse-textured soils. Catena 65, 214–221.

Kimoto, A., Nearing, M.A., Shipitalo, M.J., Polyakov, V.O., 2006b. Multi-year tracking of sediment sources in a small agricultural watershed using rare earth elements. Earth Surf. Process. Landf. 31, 1763–1774.

Kinnell, P.I.A., 2000. The effect of slope length on sediment concentrations associated with side-slope erosion. Soil Sci. Soc. Am. J. 64, 1004–1008.

Kinnell, P.I.A., 2005. Raindrop impact induced erosion processes and prediction: a review. Hydrol. Process. 19, 2815–2844.

Kinnell, P.I.A., 2009. The impact of slope length on the discharge of sediment by rain impact induced saltation and suspension. Earth Surf. Process. Landf. 34, 1393–1407.

Kirkby, M.J., 1991. Sediment travel distance as an experimental and model variable in particulate movement. In erosion, transport and deposition processes, Bork H-R, de Ploey eJ, Schick AP (eds). Catena Suppl. 19, 111–128.

Meyer, L.D., Foster, G.R., Romkens, M.J.M., 1975. Source of soil eroded by water from upland slopes. In: Present and Prospective Technology for Predicting Sediment Yields and Sources. ARS-S-40, USDA-ARS, U.S. Gov. Print. Office, Washington, DC, pp. 177–189.

Meyer, L.D., Harmon, W.C., 1989. How row-sideslope length and steepness affect sideslope erosion. Trans. ASAE 32, 639–645.

Meyer, L.D., Wischmeier, W.H., 1969. Mathematical simulation of the process of soil erosion by water. Trans. ASAE 12 (754–758), 762.

Parsons, A.J., Abrahams, A.D., Wainwright, J., 1994. Rainsplash and erosion rates in an interrill area on semi-arid grassland, Southern Arizona. Catena 22, 215–226.

Parsons, A.J., Brazier, R.E., Wainwright, J., Powell, D.M., 2006. Scale relationships in hillslope runoff and erosion. Earth Surf. Process. Landf. 31, 1384–1393.

Parsons, A.J., Wainwright, J., Abrahams, A.D., 1993. Tracing sediment movement in interrill overland flow on a semi-arid grassland hillslope using magnetic susceptibility. Earth Surf. Process. Landf. 6, 113–126.

Parsons, A.J., Wainwright, J., Powell, D.M., Kaduk, J., Brazier, R.E., 2004. A conceptual model for determining soil erosion by water. Earth Surf. Process. Landf. 29, 1293–1302.

Polyakov, V.O., Kimoto, A., Nearing, M.A., Nichols, M.H., 2009. Tracing sediment movement on a semiarid watershed using rare earth elements. Soil Sci. Soc. Am. J. 73, 1559–1565.

Polyakov, V.O., Nearing, M.A., 2004. Rare earth element oxides for tracing sediment movement. Catena 55, 255–276.

Rejman, J., Usowicz, B., Debicki, R., 1999. Source of errors in predicting silt soil erodibility with USLE. Pol. J. Soil Sci. 32, 13–22.

Singer, M.J., Walker, P.H., 1983. Rainfall-runoff in soil erosion with simulated rainfall, overland flow and cover. Aust. J. Soil Res. 21, 109–122.

Sutherland, R.A., Wan, Y., Ziegler, A.D., Lee, C.-T., El-Swaify, S.A., 1996. Splash and wash dynamics: an experimental investigation using an Oxisol. Geoderma 69, 85–103.

Tian, J.L., Zhou, P.H., Liu, P.L., 1994. REE tracer method for studies on soil erosion. Int. J. Sediment Res. 9, 39–46.

Wainwright, J., Parsons, A.J., Muller, E.N., Brazier, R.E., Powell, D.M., Fenti, B., 2008. A transport-distance approach to scaling erosion rates: I. Background and model development. Earth Surf. Process. Landf. 33, 813–826.

Young, R.A., Wiersma, J.L., 1973. The role of rainfall impact in soil detachment and transport. Water Resour. Res. 9, 1629–1636.

Zhang, X.C., Friedrich, J.M., Nearing, M.A., Norton, L.D., 2001. Potential use of rare earth oxides as tracers for soil erosion and aggregation studies. Soil Sci. Soc. Am. J. 65, 1508–1515.

Zhang, X.C., Nearing, M.A., Polyakov, V.O., Friedrich, J.M., 2003. Using rare-earth oxide tracers for studying soil erosion dynamics. Soil Sci. Soc. Am. J. 67, 279–288.

Zhang, X.C., Wang, Z.L., 2017. Interrill soil erosion processes on steep slopes. J. Hydrol. http://dx.doi.org/10.1016/j.jhydrol.2017.03.046.